

Large-scale magnetic flux concentrations from turbulent stresses

Axel Brandenburg^{1,2}, Nathan Kleeorin³, Igor Rogachevskii³

¹ NORDITA, AlbaNova University Center, Roslagstullsbacken 23, SE 10691 Stockholm, Sweden

² Department of Astronomy, AlbaNova University Center, Stockholm University, SE 10691 Stockholm, Sweden

³ Department of Mechanical Engineering, The Ben-Gurion University of the Negev, POB 653, Beer-Sheva 84105, Israel

October 25, 2018, Revision: 1.113

Key words magnetohydrodynamics (MHD) – instabilities – turbulence

In this study we provide the first numerical demonstration of the effects of turbulence on the mean Lorentz force and the resulting formation of large-scale magnetic structures. Using three-dimensional direct numerical simulations (DNS) of forced turbulence we show that an imposed mean magnetic field leads to a decrease of the turbulent hydromagnetic pressure and tension. This phenomenon is quantified by determining the relevant functions that relate the sum of the turbulent Reynolds and Maxwell stresses with the Maxwell stress of the mean magnetic field. Using such a parameterization, we show by means of two-dimensional and three-dimensional mean-field numerical modelling that an isentropic density stratified layer becomes unstable in the presence of a uniform imposed magnetic field. This large-scale instability results in the formation of loop-like magnetic structures which are concentrated at the top of the stratified layer. In three dimensions these structures resemble the appearance of bipolar magnetic regions in the Sun. The results of DNS and mean-field numerical modelling are in good agreement with theoretical predictions. We discuss our model in the context of a distributed solar dynamo where active regions and sunspots might be rather shallow phenomena.

© 0000 WILEY-VCH Verlag GmbH & Co. KGaA, Weinheim

1 Introduction

Turbulence effects generally refer to the occurrence of correlations between velocity, temperature, and/or magnetic fields at small scales. A typical example is turbulent viscosity, which results from the spatial exchange of turbulent eddies characterized by velocity correlations. This leads to the dissipation of energy at small scales.

However, there is also the possibility of additional (e.g. non-diffusive) turbulence effects, as is perhaps best known in mean-field electrodynamics and dynamo theory. Here one models the effects of the mean electromotive force, i.e. the turbulence effects of velocity and magnetic field fluctuations, on the evolution of the mean field. This can lead to the occurrence of the famous α effect, in addition to turbulent magnetic diffusion, turbulent diamagnetic velocity, etc. (Moffatt 1978; Krause & Rädler 1980). Another example is the Λ effect in rotating anisotropic hydrodynamic turbulence, which can lead to the occurrence of differential rotation in cosmic bodies such as the Sun (Rüdiger 1980, 1989; Rüdiger & Hollerbach 2004). In that case the relevant correlations come from the mean Reynolds stress tensor and its dependence on the local angular velocity.

A related example is the combined Reynolds and Maxwell turbulent stress tensor and its dependence on the mean magnetic field. The first analytic calculations of the dependence of the turbulent Reynolds stress on the mean magnetic field in the framework of the first-order smoothing approximation were performed by Rädler (1974) and Rüdiger (1976). Later, also the combined effects of the turbulent Reynolds and Maxwell stress tensors were considered (Klee-

orin et al. 1989, 1990; Rüdiger & Kichatinov 1990). It was noticed that this can lead to a local reduction of the total turbulent pressure and hence to the possibility of self-induced concentrations of large-scale magnetic fields (Kleeorin et al. 1989, 1990, 1996; Kleeorin & Rogachevskii 1994; Rogachevskii & Kleeorin 2007). Such a process may play an important role in the formation of sunspots and active regions in the Sun. It may be complementary to the magnetically induced suppression of the turbulent energy flux, which would lead to further cooling and hence a further concentration of the structures (Kitchatinov & Mazur 2000).

The current leading explanation for the formation of sunspots is related to the emergence of deeply rooted magnetic flux tubes (Parker 1955, 1982, 1984). Such flux tubes are generally believed to be produced and ‘stored’ near the bottom of the convection zone (Spiegel & Weiss 1980). The storage of magnetic fields and the formation of flux tubes in the overshoot layer near the bottom of the solar convective zone was investigated in a number of publications (see, e.g., Spruit 1981; Spruit & van Ballegooyen 1982; Schüssler et al. 1994; Moreno-Insertis et al. 1996; Tobias et al. 2001; Tobias & Hughes 2004). However, in order that the tubes retain their basic east–west orientation during their ascent over many pressure scale heights, the magnetic field must be strong enough (Choudhuri & D’Silva 1990) and is estimated to be around 10^5 G at the bottom of the convection zone (D’Silva & Choudhuri 1993). Such fields would be up to a hundred times stronger than the equipartition value, which is one of several other arguments that have led to the idea that flux emergence of dynamo-generated fields might instead be a shallow phenomenon (Brandenburg 2005; Schat-

arXiv:0910.1835v1 [astro-ph.SR] 12 Oct 2009

ten 2009). Such a scenario appears also compatible with solar subsurface flows, as inferred from local helioseismology (Zhao et al. 2001; Kosovichev 2002). In particular, Zhao et al. (2004) and Hindman et al. (2009) find the presence of converging flows around active regions at radii as large as 100–200 Mm. It appears that these convergent flows might actually be the source of the formation of active regions and perhaps sunspots rather than a consequence (Parker 1979a; Hurlburt & Rucklidge 2000). Of course, in the immediate proximity of individual spots one observes outgoing flows. Those are probably superficial, less than 1–2 Mm deep, and appear to be due to the dynamical effects of magnetoconvection in an inclined magnetic field of the penumbra (e.g., Thomas et al. 2002; Heinemann et al. 2007; Rempel et al. 2009; Kitiashvili et al. 2009).

The goal of this paper is to investigate the effects of turbulence on the mean Lorentz force by means of direct numerical simulations (DNS) for forced turbulence and to study the instability of a uniform large-scale magnetic field in an adiabatically stratified layer by means of mean-field numerical modelling based on parameterizations both of analytic formulae by Rogachevskii & Kleeorin (2007) and the results of DNS for forced turbulence. In order to study the essence of the effect, we make several simplifications by neglecting the energy equation, i.e. the specific entropy is assumed to be strictly constant in space and time. In the mean-field numerical modelling we neglect the suppression of turbulent magnetic diffusivity and turbulent viscosity, and omit correlations with density fluctuations. Nevertheless, the mean density is allowed to evolve fully self-consistently according to the usual continuity equation.

2 Turbulence effects on mean Lorentz force

Throughout this paper we adopt units for the magnetic field where the vacuum permeability is equal to unity, i.e. the magnetic pressure is given by $\frac{1}{2}\overline{\mathbf{B}^2}$.

2.1 General considerations

We use the equations of mean-field magnetohydrodynamics (MHD). These equations are obtained by averaging the original MHD equations over small-scale fluctuations. This technique is best known in the case of the induction equation (Moffatt 1978; Krause & Rädler 1980). In this study we are mainly interested in effects of turbulence on the mean Lorentz force. Let us consider the momentum equation,

$$\frac{\partial}{\partial t}\rho\mathbf{U} = -\frac{\partial}{\partial x_j}\Pi_{ij}, \quad (1)$$

where

$$\Pi_{ij} = \rho U_i U_j + \delta_{ij} \left(p + \frac{1}{2}\mathbf{B}^2 \right) - B_i B_j - \sigma_{ij} \quad (2)$$

is the momentum stress tensor, \mathbf{U} and \mathbf{B} are the velocity and magnetic fields, p and ρ are the fluid pressure and density, δ_{ij} is the unit Kronecker tensor, $\sigma_{ij} = 2\rho\nu S_{ij}$ is the viscous stress tensor, with

$$S_{ij} = \frac{1}{2}(U_{i,j} + U_{j,i}) - \frac{1}{3}\delta_{ij}\nabla\cdot\mathbf{U} \quad (3)$$

being the traceless rate of the strain tensor, and ν is the kinematic viscosity. Ignoring the turbulent correlations with density fluctuations for low-Mach number turbulence, the averaged momentum equation is

$$\frac{\partial}{\partial t}\overline{\rho\mathbf{U}} = -\frac{\partial}{\partial x_j}\overline{\Pi_{ij}}, \quad (4)$$

where $\overline{\Pi_{ij}} = \overline{\Pi_{ij}^m} + \overline{\Pi_{ij}^f}$ is the mean momentum stress tensor split into contributions resulting entirely from the mean field (indicated by superscript m) and those of the fluctuating field (indicated by superscript f). The tensor $\overline{\Pi_{ij}^m}$ has the same form as Eq. (2), but all quantities have now attained an overbar, i.e.

$$\overline{\Pi_{ij}^m} = \overline{\rho} \overline{U_i U_j} + \delta_{ij} \left(\overline{p} + \frac{1}{2}\overline{\mathbf{B}^2} \right) - \overline{B_i B_j} - \overline{\sigma_{ij}}. \quad (5)$$

We emphasize here that \overline{p} is just the mean gas pressure and $\overline{\sigma_{ij}}$ is the average of the microscopic viscous stress tensor, σ_{ij} . The contribution from the fluctuating fields, in turn, is split into contributions that are independent of the mean fields (and hence isotropic and proportional to δ_{ij}) and contributions which depend on the mean fields,

$$\overline{\Pi_{ij}^f} = p_{t0}\delta_{ij} - \sigma_{ij}^{\text{eff}}. \quad (6)$$

Here, p_{t0} is the turbulent pressure in the absence of a mean magnetic field and $\sigma_{ij}^{\text{eff}} = \sigma_{ij}^K + \sigma_{ij}^M$ quantifies the turbulent viscosity, $\sigma_{ij}^K = 2\overline{\rho\nu_t S_{ij}}$, and the additional effects of the mean magnetic field on the effective stress tensor. Both terms, $p_{t0}\delta_{ij} - \sigma_{ij}^M$, result from the fluctuations $\mathbf{u} = \mathbf{U} - \overline{\mathbf{U}}$ and $\mathbf{b} = \mathbf{B} - \overline{\mathbf{B}}$ of velocity and magnetic fields, and are given by

$$p_{t0}\delta_{ij} - \sigma_{ij}^M = \overline{\rho u_i u_j} + \frac{1}{2}\delta_{ij}\overline{\mathbf{b}^2} - \overline{b_i b_j}. \quad (7)$$

In the absence of a mean magnetic field, the turbulent background pressure is

$$p_{t0} = \frac{1}{6}\overline{\mathbf{b}_0^2} + \frac{1}{3}\rho\overline{\mathbf{u}_0^2} \quad (8)$$

where the subscripts 0 on \mathbf{b}^2 and \mathbf{u}^2 indicate values in the absence of the mean magnetic field. Magnetic fluctuations \mathbf{b} are generated both by small-scale dynamo action and by tangling of the mean magnetic field by velocity fluctuations. On the other hand, the velocity fluctuations also have two contributions, those that depend on the mean magnetic field and those that do not.

Following Rogachevskii & Kleeorin (2007), the part of the effective stress tensor that depends on the mean magnetic field is parameterized as

$$\sigma_{ij}^M(\overline{\mathbf{B}}) = -q_s \overline{B_i B_j} + \frac{1}{2}\delta_{ij} q_p \overline{\mathbf{B}^2}, \quad (9)$$

where q_s and q_p are functions of the mean field, $\overline{\mathbf{B}}$, and the magnetic Reynolds number, R_m . Eq. (9) implies that the effective mean Lorentz force that takes into account the effects of turbulence, can be written as:

$$\overline{\rho\mathcal{F}_M} = -\frac{1}{2}\nabla[(1 - q_p)\overline{\mathbf{B}^2}] + \overline{\mathbf{B}} \cdot \nabla[(1 - q_s)\overline{\mathbf{B}}]. \quad (10)$$

The detailed analytic expressions for $q_s(\overline{\mathbf{B}})$ and $q_p(\overline{\mathbf{B}})$ have been given by Rogachevskii & Kleeorin (2007). The asymptotic formulae for the nonlinear functions, $q_p(\overline{\mathbf{B}})$ and $q_s(\overline{\mathbf{B}})$,

are given below. For this purpose we define $\beta \equiv \bar{B}/B_{\text{eq}}$, where $B_{\text{eq}} = (\rho u_0^2)^{1/2}$ is the equipartition field strength.

For very weak mean magnetic fields, $4\beta \ll \text{Rm}^{-1/4}$, q_p and q_s are approximately constant and given by

$$q_p(\beta) = \frac{4}{45} (1 + 9 \ln \text{Rm}),$$

$$q_s(\beta) = \frac{2}{15} (1 + 4 \ln \text{Rm}),$$

for $\text{Rm}^{-1/4} \ll 4\beta \ll 1$ we have

$$q_p(\beta) = \frac{16}{25} [1 + 5 |\ln(4\beta)| + 32 \beta^2],$$

$$q_s(\beta) = \frac{32}{15} \left[|\ln(4\beta)| + \frac{1}{30} + 12 \beta^2 \right],$$

and for strong fields, $4\beta \gg 1$, we have

$$q_p(\beta) = 1/6\beta^2, \quad q_s(\beta) = \pi/48\beta^3.$$

(Rogachevskii & Kleeorin 2007).

In Sect. 2.2 we present DNS evidence that the functions $q_p(\bar{B})$ and $q_s(\bar{B})$ are positive, indicating the possibility of a reduction of the effective Lorentz force, i.e., a decrease of the effective magnetic pressure and magnetic tension in small-scale turbulence.

2.2 DNS of turbulence effects on mean Lorentz force

In order to study turbulence effects on the mean Lorentz force and to determine the functions $q_p(\bar{B})$ and $q_s(\bar{B})$ from DNS, we consider forced turbulence in a periodic three-dimensional domain in the presence of an imposed uniform magnetic field, say $\bar{B}_0 = (\bar{B}_0, 0, 0)$. We determine q_s and q_p from Eqs. (7) and (9) for $i = j = x$,

$$p_{t0} + \frac{1}{2}(\bar{b}_x^2 - \bar{b}_y^2 - \bar{b}_z^2) - \bar{p} \bar{u}_x^2 = (\frac{1}{2}q_p - q_s) \bar{B}_0^2, \quad (11)$$

and $i = j = y$,

$$p_{t0} + \frac{1}{2}(\bar{b}_y^2 - \bar{b}_x^2 - \bar{b}_z^2) - \bar{p} \bar{u}_y^2 = \frac{1}{2}q_p \bar{B}_0^2, \quad (12)$$

where p_{t0} is given by Eq. (8). First, we determine p_{t0} from a simulation with $\bar{B}_0 = 0$. Then, we use Eq. (12) to determine $q_p(\bar{B})$. Finally, to determine $q_s(\bar{B})$ we subtract Eq. (11) from Eq. (12), i.e.

$$(\bar{b}_y^2 - \bar{b}_x^2) - \bar{p}(\bar{u}_y^2 - \bar{u}_x^2) = q_s \bar{B}_0^2. \quad (13)$$

In order to determine separately the effects of the mean field on the turbulent Maxwell and Reynolds stresses we also compute their respective contributions $q_p^M + q_p^K = q_p$ and $q_s^M + q_s^K = q_s$. In the current case where there is no small-scale dynamo action we have

$$q_p^M = (\bar{b}_y^2 - \bar{b}_x^2 - \bar{b}_z^2) / \bar{B}_0^2, \quad q_p^K = 2(p_{t0} - \bar{p} \bar{u}_y^2) / \bar{B}_0^2, \quad (14)$$

In Fig. 1 we show the results from the simulations of forced turbulence in the presence of an imposed magnetic field. Here we have also plotted the total turbulent energy, $E_T = E_K + E_M$ where

$$E_K = \bar{p} \bar{u}^2 / 2, \quad E_M = \bar{b}^2 / 2 \quad (15)$$

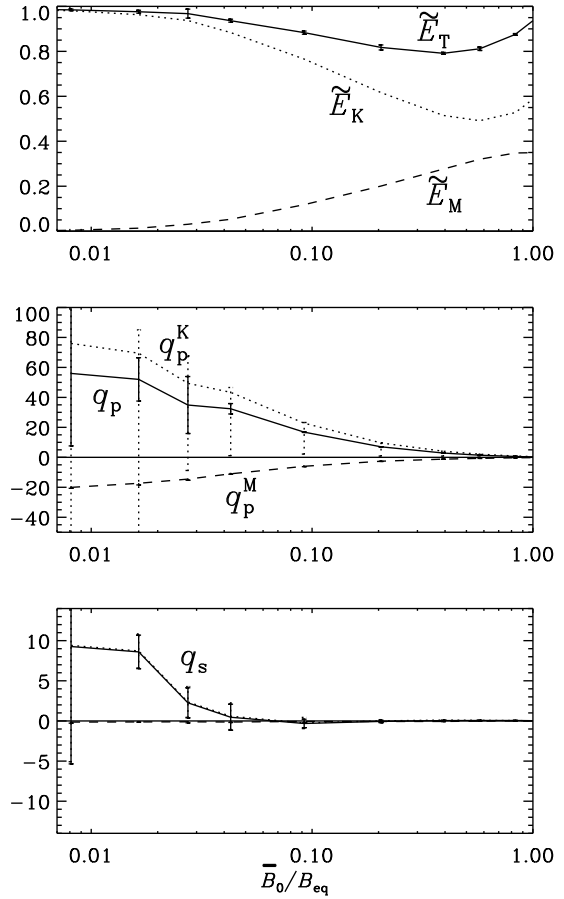


Fig. 1 \bar{B}_0 dependence of the normalized turbulent energy $\tilde{E}_T = E_T/E_0$, where E_0 is the value of E_T for $\bar{B}_0 = 0$, together with the contributions from kinetic and magnetic energies, $\tilde{E}_K = E_K/E_0$ and $\tilde{E}_M = E_M/E_0$, (upper panel) as well as the coefficients q_p , q_p^K , q_p^M , and q_s obtained from DNS for $\text{Re} = 180$ and $R_m = 45$ (second and third panels).

are the energy densities of velocity and magnetic fluctuations, respectively. The simulations were performed with the PENCIL CODE¹, which uses sixth-order explicit finite differences in space and third order accurate time stepping method. They are similar to the DNS of Haugen & Brandenburg (2004). The forcing function consists of plane non-polarized waves with an average wavenumber $k_f = 1.5 k_1$, where $k_1 = 2\pi/L$ is the smallest wavenumber that fits into a 3D periodic domain of size L . We use an isothermal equation of state with constant sound speed c_s . The forcing strength is arranged such that the turbulent rms velocity, u_{rms} , is below c_s . In all our runs the maximum turbulent Mach number, u_{rms}/c_s , is around 0.2, so that compressibility effects are still weak.

The fluid Reynolds number based on the forcing wave number $k_f = 2\pi/l_f$, is $\text{Re} = u_{\text{rms}}/\nu k_f \approx 180$ and the magnetic Prandtl number is $\nu/\eta = 0.25$, so the magnetic Reynolds number, $R_m = u_{\text{rms}}/\eta k_f \approx 45$, is just small

¹ <http://www.nordita.org/software/pencil-code/>

enough so that no small-scale dynamo is excited. [Following Haugen et al. (2004) and Schekochihin et al. (2005, 2007), the critical value of R_m is between 70 and 80 for this value of the magnetic Prandtl number]. Note that the magnetic Reynolds number, R_m , used in Sect. 2.1 is based on forcing scale $l_f = 2\pi/k_f$, and thus $R_m = 2\pi R_m$. In all cases we normalize the field strength in terms of the equipartition value, $B_{\text{eq}} = \rho_0^{1/2} u_{\text{rms}}$. The number of mesh points is 64^3 .

As follows from our DNS study, both functions $q_p(\bar{B})$ and $q_s(\bar{B})$ are positive and exceed unity for weak fields. The error bars are obtained by calculating averages over each of three equally long intervals of the full time series and taking the largest deviation from the full averages. For very small values of B_0/B_{eq} , the turbulent fluctuations dominate over the effects from shredding the imposed field, which increases the error bars. Nevertheless, the results are in agreement with the prediction of Rogachevskii & Kleeorin (2007). Note also that both theory and simulations suggest that $q_p > 2q_s$.

2.3 Physics of turbulence effects on Lorentz force

The physics of the effect of turbulence on the large-scale Lorentz force is as follows. The equation of state for isotropic turbulence is given by

$$p_{t0} = \frac{1}{3}E_M + \frac{2}{3}E_K, \quad (16)$$

[see, e.g., Landau & Lifshitz 1975, 1984, and Eq. (8)], where p_{t0} is the total (hydrodynamic plus magnetic) turbulent pressure, and E_K and E_M are defined by Eq. (15). The total energy density $E_T = E_K + E_M$ of homogeneous turbulence with a mean magnetic field \bar{B} is determined by the equation

$$\frac{\partial E_T}{\partial t} = I_T - \frac{E_T}{\tau_0} + \eta_t(\nabla \times \bar{B})^2, \quad (17)$$

where τ_0 is the correlation time of the turbulent velocity field in the maximum scale l_f of turbulent motions, I_T is the energy source of turbulence, η_t is the turbulent magnetic diffusion. For a given time-independent source of turbulence I_T and for $t \gg \tau_0$ the total energy density of the turbulence reaches a steady state

$$E_T = \text{const} = \tau_0 I_T, \quad (18)$$

where we neglect a small magnetic source $\eta_t(\nabla \times \bar{B})^2$ of the turbulence [that is of the order of $O(l_f^2/H_B^2)$, and H_B is the characteristic scale of the mean magnetic field spatial variations]. The approximate constancy of E_T is compatible with DNS, where we found only a small decrease (20%) for strong (equipartition strength) mean fields (see the upper panel of Fig. 1). The reason for the departure is possibly a dependence of τ_0 on \bar{B} . However, this decrease only enhances the modification of the Lorentz force by turbulence.

Equations (16) and (18) imply that the change of turbulent pressure δp_{t0} is proportional to the change of the magnetic energy density δE_M , in particular $\delta p_{t0} = -(1/3)\delta E_M$ (because $\delta E_K = -\delta E_M$). Therefore, the total turbulent

pressure is reduced when magnetic fluctuations are generated.

For a non-zero large-scale mean magnetic field \bar{B} , the change of the magnetic energy density δE_M is proportional to \bar{B}^2 . Therefore, the total turbulent pressure is given by $P_t = p_{t0} - \frac{1}{2}q_p\bar{B}^2$, where p_{t0} is the turbulent pressure in a flow with a zero mean magnetic field. The coefficient $q_p > 0$ when magnetic fluctuations are generated. Now we examine the part, $P_{\text{eff}}(\bar{B})$, of the total pressure, $P_{\text{tot}} = \bar{p} + P_t + \frac{1}{2}\bar{B}^2$, that depends on the mean magnetic field, \bar{B} , i.e., we consider the effective mean magnetic pressure that takes into account the contribution of turbulence, $P_{\text{eff}}(\bar{B}) = \frac{1}{2}(1 - q_p)\bar{B}^2$. We study the case when $\bar{p} \gg \bar{B}^2/2$, and therefore, the total pressure P_{tot} is always positive, while the effective mean magnetic pressure $P_{\text{eff}}(\bar{B})$ may be negative when $q_p > 1$.

The modification of the mean Lorentz force can result in the excitation of a long wavelength instability even in an initially uniform mean magnetic field in a density stratified layer (Kleeorin et al. 1990, 1996; Rogachevskii & Kleeorin 2007). Indeed, the growth rate of the instability for the perturbations perpendicular to both the gravity field \mathbf{g} and the mean magnetic field \bar{B} is given by

$$\lambda = \frac{c_a}{H_\rho} \sqrt{(1 - q_p) \left(\frac{H_\rho}{H_B} - 1 \right)}, \quad (19)$$

where $c_a = \bar{B}/\rho_0^{1/2}$ is the Alfvén speed, $H_\rho^{-1} = |\nabla \ln \rho_0|$, $H_B^{-1} = |\nabla \ln \bar{B}|$, and we neglected for simplicity the dissipation processes due to turbulent viscosity and turbulent magnetic diffusion. For $q_p > 1$ the instability is excited when $H_\rho < H_B$, i.e., it occurs even in an initially uniform mean magnetic field.

The mechanism of the instability can be understood as follows. An isolated magnetic tube moving upward becomes lighter than the surrounding plasma since the decrease of the magnetic field in it, due to expansion of the tube, is accompanied with an increase of the magnetic pressure inside the tube. This increase, due to the fact that the effective magnetic pressure is negative, leads to a decrease of the density inside the tube and to the appearance of a buoyancy force. It results in the further upward displacement of the flux tube, i.e. it causes the excitation of the instability. The instability causes the formation of inhomogeneous magnetic structures. The energy for this instability is supplied by the small-scale turbulence. In contrast, the free energy in Parker's magnetic buoyancy instability, that is excited when $H_\rho > H_B$, is drawn from the gravitational field (Newcomb 1961; Parker 1966). The growth rate of Parker's magnetic buoyancy instability is determined by Eq. (19) for $q_p = 0$.

Magnetic buoyancy in astrophysics applies usually to two different situations (see, e.g., Priest 1982). The first corresponds to a problem described by Parker (1966, 1979b) and Gilman (1970a, 1970b). They considered the instability of a stratified continuous magnetic field and did not invoke a magnetic flux tube. The other situation was considered

by Parker (1955), Spruit (1981), Spruit & van Ballegoijen (1982), Ferriz-Mas & Schüssler (1993), and Schüssler et al. (1994), who studied buoyancy of horizontal magnetic flux tubes.

In the present study we investigate the first situation, i.e., we study the large-scale instability of a continuous (diffusive) magnetic field in small-scale turbulence. This instability is caused by turbulent velocity and magnetic fluctuations and leads to the formation of large-scale magnetic structures (see Sect. 3).

3 Mean-field numerical modelling

In order to understand in more detail the appearance of magnetic structures from this large-scale instability we consider now numerical solutions of the mean-field MHD equations in a density stratified layer. We apply a new mean-field model which includes the effect of turbulence on mean Lorentz force. We solve the evolution equations for mean velocity $\overline{\mathbf{U}}$, mean density $\overline{\rho}$, and mean vector potential $\overline{\mathbf{A}}$ in the form

$$\frac{\partial \overline{\mathbf{U}}}{\partial t} = -\overline{\mathbf{U}} \cdot \nabla \overline{\mathbf{U}} - c_s^2 \nabla \ln \overline{\rho} + \mathbf{g} + \overline{\mathcal{F}}_{\mathbf{M}} + \overline{\mathcal{F}}_{\mathbf{K},\text{tot}}, \quad (20)$$

$$\frac{\partial \ln \overline{\rho}}{\partial t} = -\overline{\mathbf{U}} \cdot \nabla \ln \overline{\rho} - \nabla \cdot \overline{\mathbf{U}}, \quad (21)$$

$$\frac{\partial \overline{\mathbf{A}}}{\partial t} = \overline{\mathbf{U}} \times \overline{\mathbf{B}} - (\eta_t + \eta) \overline{\mathbf{J}}, \quad (22)$$

where $\overline{\mathcal{F}}_{\mathbf{M}}$ is given by Eq. (10), and $\overline{\mathcal{F}}_{\mathbf{K},\text{tot}} = \overline{\mathcal{F}}_{\mathbf{K}} + \overline{\mathcal{F}}_{\text{visc}}$ with $\overline{\rho} \overline{\mathcal{F}}_{\mathbf{K}} = \nabla \cdot \sigma^{\mathbf{K}}$ and with $\overline{\rho} \overline{\mathcal{F}}_{\text{visc}} = \nabla \cdot \overline{\sigma}$, so that

$$\overline{\mathcal{F}}_{\mathbf{K},\text{tot}} = (\nu_t + \nu) (\nabla^2 \overline{\mathbf{U}} + \nabla \nabla \cdot \overline{\mathbf{U}} + 2 \overline{\mathbf{S}} \nabla \ln \overline{\rho}) \quad (23)$$

is the total (turbulent and microscopic) viscous force and \mathbf{S} is given by Eq. (3).

We consider two- and three-dimensional models of an isentropically stratified atmosphere, where the gravitational potential is written as $\Phi(z) = (z - z_\infty)g$, so the gravity vector $\mathbf{g} = -\nabla \Phi = (0, 0, -g)$ is constant. We arrange the initial profiles of density and sound speed such that they take given reference values at $z = 0$, i.e. $\overline{\rho} = \rho_0$ and $c_s = c_{s0}$ at $z = 0$. This implies that $z_\infty = (3/2)c_{s0}^2/g$. Our initial profiles therefore obey

$$\rho/\rho_0 = (c_s/c_{s0})^3, \quad c_s^2 = -\frac{2}{3}\Phi. \quad (24)$$

The local density scale height is $H_\rho = c_s^2/g$, and the density scale height at $z = 0$ is $H_{\rho 0} = c_{s0}^2/g$. In Fig. 2 we show the vertical dependence of the initial density.

We allow for the presence of an imposed field in the y direction, $\mathbf{B}_0 = (0, B_0, 0)$. The total field is then written as $\overline{\mathbf{B}} = \mathbf{B}_0 + \nabla \times \overline{\mathbf{A}}$, (25)

so the departure from the imposed field is expressed in terms of the mean magnetic vector potential $\overline{\mathbf{A}}$.

On the upper and lower boundaries we adopt stress-free boundary conditions for velocity, i.e. $\overline{U}_{x,z} = \overline{U}_{y,z} = \overline{U}_z = 0$, and a normal-field condition for the magnetic field, i.e. $\overline{B}_x = \overline{B}_y - B_0 = 0$, corresponding to $\overline{A}_{x,z} = \overline{A}_{y,z} =$

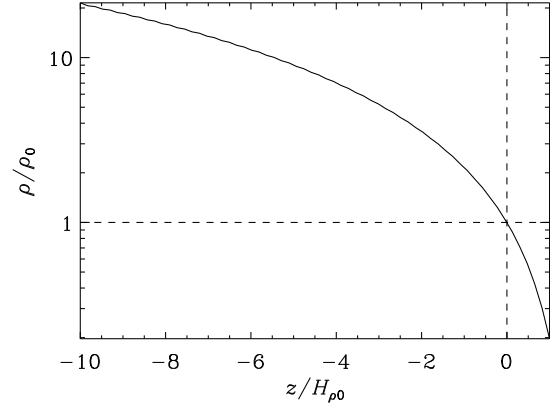


Fig. 2 Density stratification in a model with $z_{\text{top}} = H_{\rho 0}$. The dashed lines indicate the reference value with $\rho = \rho_0$ at $z = 0$.

$\overline{A}_z = 0$ for the vector potential. Here, commas denote partial differentiation. No boundary condition for the density is required. Again, all computations have been carried out with the PENCIL CODE.

In setting up our model we define the wavenumber k_f of the energy-carrying eddies. This relates the turbulent magnetic diffusivity to the rms velocity via $\eta_t = u_{\text{rms}}/3k_f$. This means that the ratio of our non-dimensional field strength to turbulent diffusivity, i.e. $B_0/c_{s0}\rho_0^{1/2}$ to $\eta_t/c_{s0}H_\rho$, is given by $3k_f H_0$ times B_0/B_{eq} .

In this paper we approximate q_p and q_s by simple profile functions,

$$q_p = q_{p0} \left(1 - \frac{2}{\pi} \arctan \frac{\overline{\mathbf{B}}^2}{\overline{B}_p^2} \right), \quad (26)$$

$$q_s = q_{s0} \left(1 - \frac{2}{\pi} \arctan \frac{\overline{\mathbf{B}}^2}{\overline{B}_s^2} \right). \quad (27)$$

Following Rogachevskii & Kleeorin (2007), we also define $Q_p = 1 - q_p$ and $Q_s = 1 - q_s$. Correspondingly, we define the coefficients $Q_{p0} = 1 - q_{p0}$ and $Q_{s0} = 1 - q_{s0}$. For our fiducial model we use $Q_{p0} = 2Q_{s0} = 20$, corresponding to $q_{p0} = 21$ and $q_{s0} = 11$. The resulting magnetic pressure is shown in Fig. 3 for their analytic theory and the result from DNS is shown in Fig. 4, together with the corresponding fits. For our fiducial model we choose furthermore $\overline{B}_p = \overline{B}_s = 0.1 c_{s0}\rho_0^{1/2}$. For the imposed field strength we choose $B_0/c_{s0}\rho_0^{1/2} = 0.01$ and for the turbulent magnetic diffusivity we take $\eta_t/c_{s0}H_\rho = 0.01$. As discussed above, this means that $B_0/B_{\text{eq}} = 1/3$ if we assume $k_f H_0 = 1$.

3.1 Magnetic structures in two-dimensions

In this paper we consider both two-dimensional and three-dimensional solutions. We begin with two-dimensional models in the xz plane with an imposed field in the normal (y) direction, $\mathbf{B}_0 = (0, B_0, 0)$.

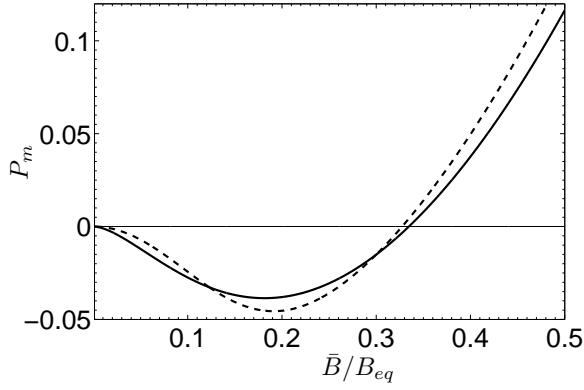


Fig. 3 The effective mean magnetic pressure $P_m(\bar{B}) = (1 - q_p)\bar{B}^2/\bar{B}_p^2$ determined by Rogachevskii & Kleeorin (2007) – solid line, and by the model described by Eq. (26) – dashed line ($\bar{B}_p = 0.21 c_{s0}\rho_0^{1/2}$ and $q_{p0} = 4$).

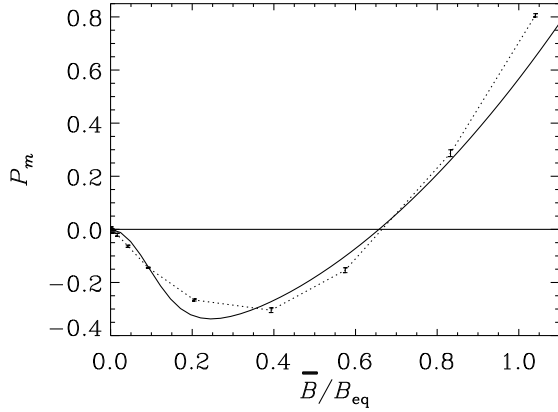


Fig. 4 Same as Fig. 3, but from simulation (dotted line). The solid line shows a fit [Eq. (26)] with $\bar{B}_p = 0.022 c_{s0}\rho_0^{1/2}$ (corresponding to $\bar{B}_p/B_{eq} = 0.18$) and $q_{p0} = 21$.

In Table 1 we present a summary of some exploratory runs where we list the nondimensional growth rate $\tilde{\lambda} \equiv \lambda H_\rho^2/\eta_t$, as well as the nondimensional saturation values of rms mean velocity and mean magnetic field, $\tilde{U}_{rms} \equiv \bar{U}_{rms}H_{\rho 0}/\eta_t$ and $\tilde{B}_{rms} \equiv \bar{B}_{rms}H_{\rho 0}/\eta_t\rho_0^{1/2}$. These experiments show that decreasing Q_{p0} and Q_{s0} lowers the growth rate and the saturation values, while increasing the degree of stratification (e.g., increasing $\tilde{z}_{top} \equiv z_{top}/H_{\rho 0}$ from 1 to 1.2, corresponding to an increase of bottom to top density ratio from 108 to 237) enhances them. Likewise, increasing the strength of the imposed field enhances the growth rate and the saturation values, while increasing the magnetic diffusivity lowers them. These results are in agreement with Eq. (19).

In Fig. 5 we compare the evolution of the rms values of velocity and magnetic field for two different stratifications. As discussed above, increasing the amount of stratification

Table 1 Summary of non-dimensional run parameters together with the resulting non-dimensional growth rates $\tilde{\lambda}$ as well as the non-dimensional saturation values of rms velocity and magnetic field. The tildes indicate non-dimensional quantities, as explained in Sect. 3.1. Our fiducial run is Run C.

	\tilde{B}_0	$\tilde{\eta}_t$	\tilde{z}_{top}	Q_{p0}	Q_{s0}	$\tilde{\lambda}$	\tilde{U}_{sat}	\tilde{B}_{sat}
A	0.01	0.01	1	-4	-2	0.0005	0.000	0.000
B	0.01	0.01	1.2	-20	-10	0.012	0.013	0.013
C	0.01	0.01	1	-20	-10	0.006	0.013	0.013
D	0.02	0.01	1	-20	-10	0.032	0.025	0.026
E	0.01	0.02	1	-20	-10	0.001	0.001	0.010

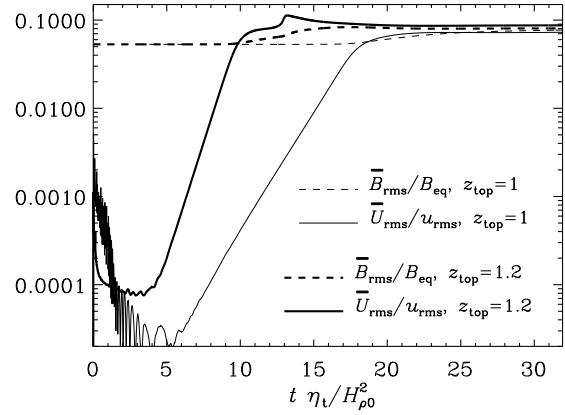


Fig. 5 Growth of the rms value of mean velocity and mean magnetic field for two runs with different degree of stratification.

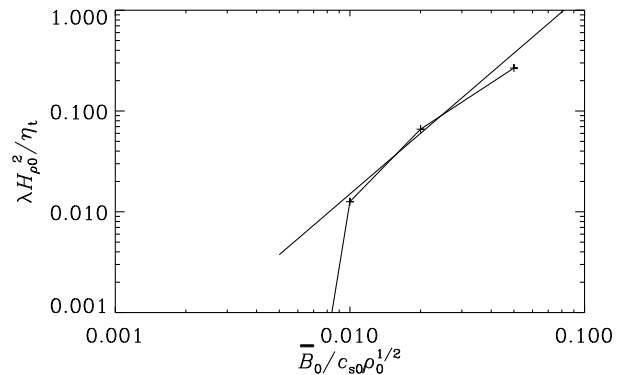


Fig. 6 Growth rate as a function of B_0 , keeping all other parameters as for the fiducial Run C.

increases the growth rate. The scaling of the growth rate with the strength of the imposed field is shown in Fig. 6.

Next, we consider the structure of the resulting magnetic field. In Fig. 7 we show “meridional” (xz) cross-sections of

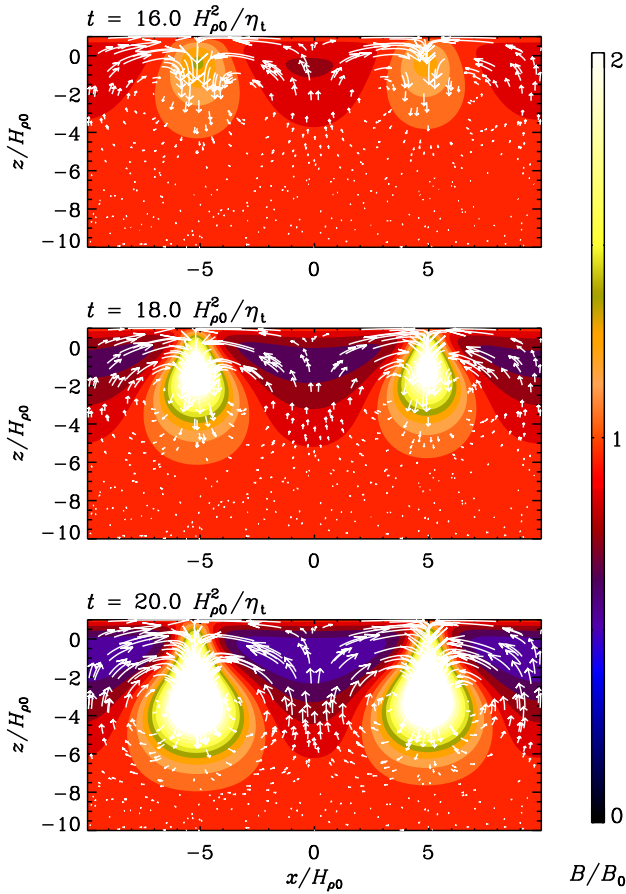


Fig. 7 Early evolution of magnetic field in the y direction (color coded) together with velocity vectors in the xz plane. Note the spontaneous production of flux structures.

the magnetic field at three different times during the early phase where the magnetic field just begins to saturate. The horizontal wavelength of the pattern is about $10 H_\rho$. As time goes on, the structures of enhanced magnetic field intensify. The decrease of the effective pressure makes them even heavier which explains their subsequent descent.

At later times new structures can form near the surface. In Fig. 8 we show an example during the fully saturated phase of the instability, where one sees the emergence of a new patch that is then swept to the larger one and merges.

3.2 Magnetic structures in three-dimensions

In order to demonstrate the three-dimensional nature of the instability we extend the domain in the y direction, so both x and y are between $\pm 10 H_\rho$, and $-10 \leq z/H_\rho \leq 1$. These simulations are otherwise similar to those in the two-dimensional cases. In Fig. 9 we show visualizations of the field at three characteristic times. Note in particular that the wavelength of the pattern in the y direction (parallel to the field) is 3–4 times shorter than that in the x direction (perpendicular to the field). Again, the instability begins to emerge first near the surface where it develops magnetic structures which begin to sink downwards. Viewed from

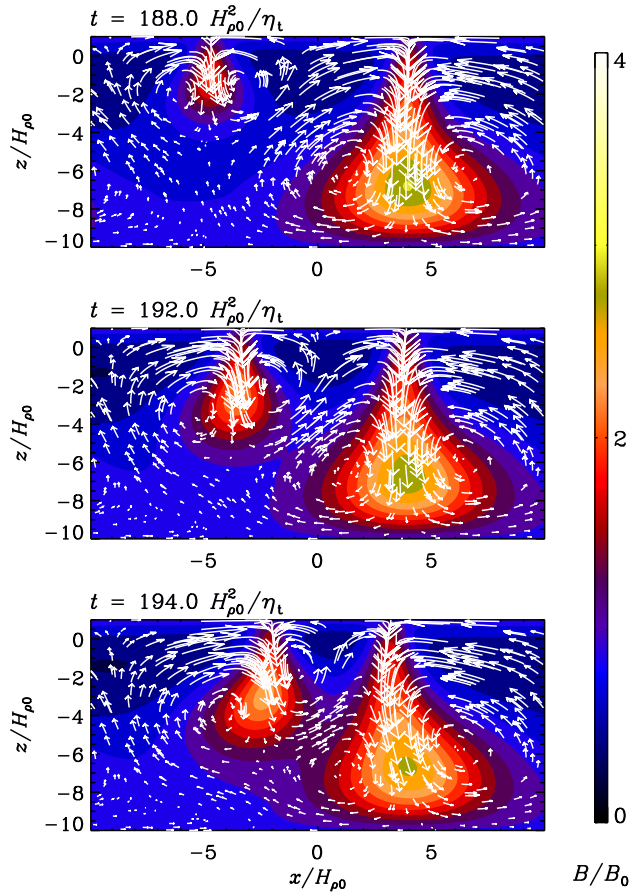


Fig. 8 Later evolution of magnetic field for the same run as in Fig. 7. Note the mutual merging of flux structures.

above, one sees the emergence of what looks like multiple bipolar regions.

In Fig. 10 we show a horizontal cross-section from another simulation, where the horizontal extent is only half as much as before. This figure is suggestive of the formation of bipolar structures. The plane has been rotated by 90° such that the y direction points now from left to right. The black horizontal bar gives the density scale height at the depth of the cross-section, which is about twice the value H_ρ at the reference depth.

4 Conclusions

In this study we have demonstrated in DNS the effects of turbulence on the mean Lorentz force. This effect is quantified by determining the relevant functions $q_p(\overline{\mathbf{B}})$ and $q_s(\overline{\mathbf{B}})$ that relate the sum of the turbulent Reynolds and Maxwell stresses with the Maxwell stress of the mean magnetic field. Using three-dimensional simulations of forced hydromagnetic turbulence with an imposed field, we confirm that the function $q_p(\overline{\mathbf{B}})$ is positive and can reach values much larger than unity for $\overline{B}/B_{\text{eq}} \ll 1$. This thereby reverses the sign of the effective magnetic pressure $P_{\text{eff}}(\overline{\mathbf{B}})$ associated with the mean magnetic field, which then becomes $P_{\text{eff}}(\overline{\mathbf{B}}) =$

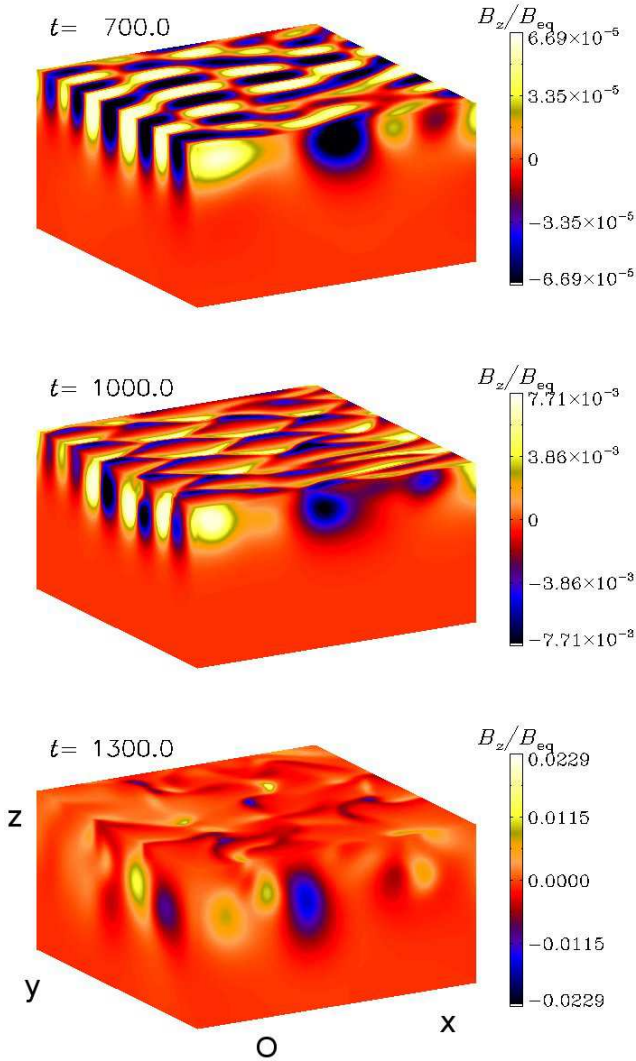


Fig. 9 Visualizations of the magnetic field at the early saturation phase ($t = 700 H_{\rho 0}/c_{s0} = 7 H_{\rho 0}^2/\eta t$ left), at an intermediate time ($t = 1000 H_{\rho 0}/c_{s0} = 10 H_{\rho 0}^2/\eta t$ left), and a later time ($t = 1300 H_{\rho 0}/c_{s0} = 13 H_{\rho 0}^2/\eta t$ left). Note the broad similarity of field in the xz plane with the two-dimensional cases. Note that the wavelength of the pattern is shorter in the y direction than in the x direction. In the final time much of the magnetic field structures have sunk beneath the surface, leaving only a few isolated bipolar structures at the surface.

$\frac{1}{2}(1 - q_p)\overline{B}^2$. We find that the function $q_s(\overline{B})$ that determines the modification of magnetic tension, also reaches values much larger than unity, but its value is less than half the value of q_p and the error bars are larger. This work has also demonstrated explicitly the possibility of a large-scale instability of the full system of mean-field MHD equations. Finally, our study has revealed the presence of spatial structures arising from the instability that might be associated with the formation of bipolar magnetic regions and perhaps also sunspots when applied to the Sun.

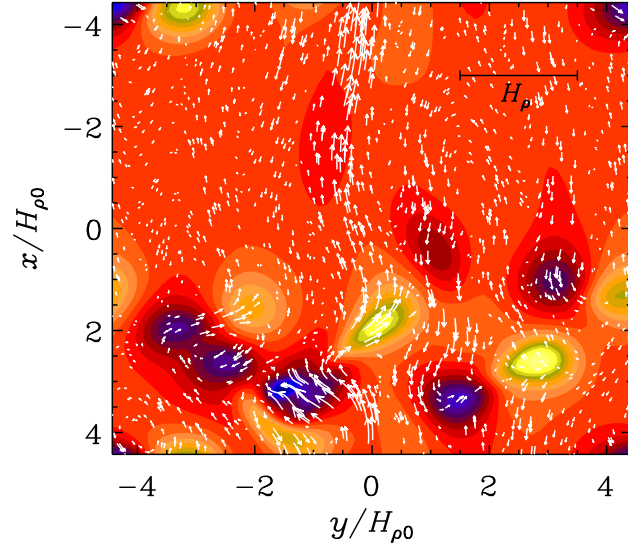


Fig. 10 Magnetic field in the xy plane. Note that the plane has been rotated by 90° in the counterclockwise direction, so the y direction, corresponding to the azimuthal direction when applied to the Sun, points from left to right. The black horizontal bar gives the density scale height at the depth of the cross-section, which is about twice the value $H_{\rho 0}$ at the reference depth.

The effects of turbulence on the large-scale Lorentz force may also be important in applications to the solar torsional oscillations by changing the mean magnetic tension $\overline{\mathbf{B}} \cdot \nabla \overline{\mathbf{B}}$ (Rüdiger et al. 1986; Rüdiger & Kichatinov 1990). More specifically, these turbulence effects may be critical for explaining the narrow structure of the observed solar torsional oscillations (Kleeorin et al. 1996).

Clearly, there are several possibilities of improvement that might make the model more realistic and eventually suitable for confrontation against observations. Most important is perhaps the fact that our reference values B_{p0} and B_{s0} in the quenching profiles (26) and (27), as well as the coefficients q_{p0} and q_{s0} in these profile functions, are currently kept constant. It will be more realistic to make them vary with depth, because density and turbulent rms velocity vary with depth. Another extension of the model would be to allow for the possibility that the magnetic field to be generated by a mean-field dynamo rather than relying on an imposed field.

On the more theoretical side, there is a need to further verification of the essential physics of the negative magnetic pressure effect. In particular, one must wonder why the effects of this instability have not yet seen in DNS. A likely possibility is the lack of sufficient scale separation. Only now realistic simulations are beginning to be large enough to encompass sufficiently many cells in all three directions. The importance of sufficient horizontal extent was already emphasized by Tao et al. (1998), who find clear ev-

idence of a segregation into strongly magnetized and weak magnetized regions, a phenomenon that might be closely related to that reported here. A particularly promising approach might be to generalize the direct simulations discussed in the present paper to the case with vertical density stratification such that the setup becomes similar to the mean field models that we also studied in this paper. The turbulence would then still be driven by a forcing function. Another possibility is to study this effect with turbulent convection instead of forced turbulence. This is particularly interesting, because theoretical predictions of Rogachevskii & Kleeorin (2007) suggest that the modification of the effective Lorentz force will be even stronger in turbulent convection.

Acknowledgments

We have benefited from very useful discussions with Alexander Kosovichev. We acknowledge the use of computing time at the Center for Parallel Computers at the Royal Institute of Technology in Sweden as well as the National Supercomputing Center in Linköping. This work was supported in part by the European Research Council under the AstroDyn Research Project 227952 and the Swedish Research Council grant 621-2007-4064. NK and IR thank NORDITA for hospitality and support during their visits. The final stage of this work was completed while participating at the NORDITA program on “Solar and stellar dynamos and cycles”.

References

- Brandenburg, A. 2005, *ApJ*, 625, 539
 Choudhuri, A.R., D’Silva, S. 1990, *A&A*, 239, 326
 D’Silva, S., Choudhuri, A.R. 1993, *A&A*, 272, 621
 Ferriz-Mas A., Schüssler, M.: 1993, *Geophys. Astrophys. Fluid Dyn.* 72, 209
 Gilman P.A. 1970a, *ApJ*, 162, 1019
 Gilman P.A. 1970b, *A&A*, 286, 305
 Haugen, N.E.L., Brandenburg, A. 2004, *Phys. Rev.*, E 70, 036408
 Haugen, N.E.L., Brandenburg, A., Dobler, W. 2004, *Phys. Rev.*, E 70, 016308
 Heinemann, T., Nordlund, Å., Scharmer, G.B., Spruit, H.C. 2007, *ApJ*, 669, 1390
 Hindman, B.W., Haber, D.A., Toomre, J. 2009, *ApJ*, 698, 1749
 Hurlburt, N.E., Rucklidge, A.M. 2000, *MNRAS*, 314, 793
 Kitchatinov, L.L., Mazur, M.V. 2000, *Solar Phys.*, 191, 325
 Kitiashvili, I.N., Kosovichev, A.G., Wray, A.A., Mansour, N.N. 2009, *ApJ*, 700, 178
 Kleeorin, N., Mond, M., Rogachevskii, I. 1996, *A&A*, 307, 293
 Kleeorin, N., Rogachevskii, I. 1994, *Phys. Rev. E*, 50, 2716
 Kleeorin, N.I., Rogachevskii, I.V., Ruzmaikin, A.A. 1989, *Sov. Astron. Lett.*, 15, 274
 Kleeorin, N.I., Rogachevskii, I.V., Ruzmaikin, A.A. 1990, *Sov. Phys. JETP*, 70, 878
 Kosovichev, A.G. 2002, *Astron. Nachr.*, 323, 186
 Krause, F., Rädler, K.-H. 1980, *Mean-field magnetohydrodynamics and dynamo theory* (Pergamon Press, Oxford)
 Landau, L.D., Lifshitz, E.M. 1975, *Classical Theory of Fields* (Pergamon, Oxford)
 Landau, L.D., Lifshitz, E.M. 1984, *Theory of Elasticity* (Pergamon, Oxford)
 Moffatt, H.K. 1978, *Magnetic field generation in electrically conducting fluids* (Cambridge University Press, Cambridge)
 Moreno-Insertis, F. 1986, *A&A*, 166, 291
 Newcomb, W.A. 1961, *Phys. Fluids*, 4, 391
 Parker, E.N. 1955, *ApJ*, 121, 491
 Parker, E.N. 1966, *ApJ*, 145, 811
 Parker, E.N. 1979a, *ApJ*, 230, 905
 Parker, E.N. 1979b, *Cosmical magnetic fields* (Oxford University Press, New York)
 Parker, E.N. 1982, *ApJ*, 256, 302
 Parker, E.N. 1984, *ApJ*, 283, 343
 Priest, E. R. 1982, *Solar Magnetohydrodynamics* (D. Reidel Publ. Co., Dordrecht)
 Rädler, K.-H. 1974, *Astron. Nachr.*, 295, 265
 Rempel, M., Schüssler, M., Cameron, R.H., Knölker, M. 2009, *Science*, 325, 171
 Rogachevskii, I., Kleeorin, N. 2007, *Phys. Rev. E*, 76, 056307
 Rüdiger, G. 1976, *Astron. Nachr.*, 295, 275
 Rüdiger, G. 1980, *Geophys. Astrophys. Fluid Dyn.*, 16, 239
 Rüdiger, G. 1989, *Differential rotation and stellar convection: Sun and solar-type stars* (Gordon & Breach, New York)
 Rüdiger, G., Hollerbach, R. 2004, *The magnetic universe* (Wiley-VCH, Weinheim)
 Rüdiger, G., Kichatinov, L.L. 1990, *A&A*, 236, 503
 Rüdiger, G., Tuominen, I., Krause, F., Virtanen, H. 1986, *A&A*, 166, 306
 Schatten, K.H. 2009, *Solar Phys.*, 255, 3
 Schekochihin, A.A., Haugen, N.E.L., Brandenburg, A., Cowley, S.C., Maron, J.L., McWilliams, J.C. 2005, *ApJ*, 625, L115
 Schekochihin, A.A., Iskakov, A.B., Cowley, S.C., McWilliams, J.C., Proctor, M.R.E., Yousef, T.A.: 2007, *New J. Phys.*, 9, 300
 Schüssler, M., Caligari P., Ferriz-Mas A., Moreno-Insertis F. 1994, *A&A*, 281, L69
 Spiegel, E.A., Weiss, N.O. 1980, *Nature*, 287, 616
 Spruit, H.C. 1981, *A&A*, 98, 155
 Spruit, H.C., van Ballegooyen, A.A. 1982, *A&A*, 106, 58
 Tao, L., Weiss, N.O., Brownjohn, D.P., Proctor, M.R.E. 1998, *ApJ*, 496, L39
 Thomas, J.H., Weiss, N.O., Tobias, S.M., Brummell, N.H.: 2002, *Nature*, 420, 390
 Tobias, S.M., Brummell, N.H., Clune T.L., Toomre, J. 2001, *ApJ*, 549, 1183
 Tobias, S.M., Hughes, D.W. 2004, *ApJ*, 603, 785
 Zhao, J., Kosovichev, A.G. 2004, *ApJ*, 603, 776
 Zhao, J., Kosovichev, A.G., Duvall, T. 2001, *ApJ*, 557, 384